Original Article
Food Science and Technology

ISSN 0101-2061 (Print)
ISSN 1678-457X (Online)

DOI: https://doi.org/10.1590/fst.100922

Structural characterization and stability of microencapsulated flavonoids from *Lycium barbarum* L. leaves

Yanli FAN[1]*, Yufang PEI[1], Jinghua CHEN[1], Xiaotong ZHA[1], Yuxing WU[1]

Abstract

Lycium barbarum L. leaves are rich in flavonoids, which have been proven to show poor stability and solubility in the external and gastrointestinal environment. To improve the stability and water-solubility of *Lycium barbarum* L. leaves flavonoids (LBLF), sodium alginate (SA) and chitosan (CS) were utilized as the wall materials to prepare the microcapsules of LBLF (M-LBLF) by polyelectrolyte cross-linking method. The spectrum of Fourier Transform Infrared spectroscopy (FT-IR) showed M-LBLF had an absorption peak at 1735 cm^{-1}, which might be the electrostatic interaction between the positive and negative charges of SA and CS. X-ray diffraction (XRD) spectrum showed the diffraction peak at $2\theta = 51.8°$ was due to the microencapsulation and transformation of the amorphous structural part into a crystalline state. As demonstrated by Differential Scanning Calorimetry (DSC), the M-LBLF displayed wider and higher endothermic peaks due to the electrostatic interaction between SA and CS. The release of main monomers from M-LBLF in different stages of the *in vitro* digestion were detected, and it was shown that M-LBLF could resist the digestion in simulated oral fluid (SOF) and gastric fluid (SGF), and enhance the slow-release ability of LBLF in simulated intestinal fluid (SIF), indicating that microencapsulation can improve the stability of LBLF and play a slow-release role.

Keywords: flavonoid; *Lycium barbarum* L. leaves; microencapsulation; structural characterization; stability.

Practical Application: Microencapsulation greatly enhanced the stability of flavonoids and played a sustained release role, which provides a method for the application of *Lycium barbarum* L. leaves flavonoids as a functional food ingredient.

1 Introduction

Lycium barbarum L. leaves have been widely used as functional tea, medicinal vegetables, and herbal drugs in China, Southeast Asia and North America (Feng et al., 2019). It is rich in nutrients such as proteins, polysaccharides, amino acids, minerals and other nutrients, as well as natural active ingredients such as flavonoids, terpenoids, betaine, atropine, etc. (Lei et al., 2022; Lu et al., 2019). *Lycium barbarum* L. leaves have a variety of benefits such as alleviating mineral deficiency, combating heat distress, quenching thirst, and enhancing eyesight, and have been widely used as tea, vegetables and medicines (Huang et al., 2022; Mocan et al., 2017). Zhao et al. (2019) analyzed major phenolics in the *Lycium barbarum* L. leaves, including chlorogenic acid, caffeic acid, *p*-coumaric acid and ferulic acid (Zhao et al., 2019). Phenolic compounds as important active ingredients in natural plants, have various physiological activities such as antioxidative activity (Shang et al., 2022), anti-obesity (Magiera & Zaręba, 2015; Oliveira et al., 2022), anti-hypertension, anti-cancer and anti-inflammation (Cao et al., 2021). The functional stability of the flavonoids could be susceptible to environmental factors, for example oxygen, light, temperature and moisture (Hiew et al., 2022). They have poor stability in the external or gastrointestinal environment, resulting in low bioavailability and waste of resources, which hinders the high-quality development of the *Lycium barbarum* L. leaves (Lei et al., 2022). Despite the potential health benefits of flavonoids, their poor stability and insolubility are obstacles to the development of the food industry. Moreover, flavonoids degrade in gastric juice's extreme acidic pH, resulting in low bioavailability and absorption (Yousefi et al., 2020). Microencapsulation is a common delivery system, it seems that encapsulation can protect flavonoids from damage *in vivo* and *in vitro* (Wen et al., 2022).

In previous studies, we found flavonoids were unstable digestion *in vivo* and *in vitro* (Chen et al., 2020), so microencapsulation technology was selected to overcome these drawbacks. M-LBLF was created using vacuum freeze-drying technology and polyelectrolyte crosslinking with LBLF serving as the core material and SA and CS serving as the composite wall materials. Its microstructure was characterized, and its impact on the stability of gastrointestinal digestion release was compared and examined. This study analyzes the structure and stability of flavonoid microcapsules in *Lycium barbarum* L. leaves, which provide a solution for the application of flavonoids from *Lycium barbarum* L. leaves as a raw material for functional foods.

2 Materials and methods

2.1 Materials

Lycium barbarum L. leaves were purchased from Yu Xin Wolfberry Planting Co. LTD (Yinchuan China). SA and CS (≥ 98.0%)

Received 18 Aug., 2022
Accepted 19 Oct., 2022
[1]*School of Food & Wine, Ningxia University, Yinchuan, Ningxia, China*
*Corresponding author: fanyanli.nxu @qq.com

were purchased from Ryon Biotechnology Technology Co. LTD (Shanghai China). Saliva amylase, pepsin, trypsin and bile were obtained from McLean Biotechnology Co. LTD (Shanghai, China). Rutin, quercetin, karmatol, chlorogenic acid, caffeic acid, *p*-coumaric acid and ferulic acid (≥ 98.0%) were obtained from Dalian Milano Biotechnology Co. LTD (Dalian, China).

2.2 Methods

Extraction and purification of LBLF

The extraction and purification of LBLF were consistent with the method in Chen et al. (2020).

Preparation of the microencapsulated LBLF

The optimal preparation process was as follows: SA solution with a mass fraction of 2% was mixed with LBLF solution according to the core wall ratio (1:2) and stirred in the water bath at 40°C for 30 min. Then mix 2% CS solution with 5% $CaCl_2$ solution, adjust pH to 7 and keep the volume to 50 mL; the mixture of the SA and LBLF was slowly dropped into the mixture of CS and $CaCl_2$ (20 drops/min). The mixture was stirred at low speed and homogenized for 30 min, then stood for 20 min, filtered and separated. The filter residue was collected and M-LBLF were obtained through freeze-drying.

Determination of Total Flavonoid Content (TFC) and Encapsulation Efficiency (EE)

The TFC of LBLF and M-LBLF were measured using a colorimetric method at 517 nm described by Chen et al. (Chen et al., 2020). TFC was expressed by rutin equivalent (RE) weight per gram of dry extract (mg RE/g DW). 1 g of M-LBLF was dissolved in 50% ethanol (10 mL) and treated with ultrasonic for 30 min, then dilute the supernatant to 25 mL to determine the content of flavonoids A_1 (mg RE/g DE). Using 100% ethanol as solvent (the method was the same as above), the content of flavonoid A_0 (mg RE/g DE) was determined. The EE was calculated by the following formula (Equation 1).

$$EE(\%) = \left(\frac{A_1 - A_0}{A_0}\right) \times 100 \quad (1)$$

Process optimization of microcapsule preparation

Based on the single factor test, the Plackett Burman test design was carried out using Design Expert 11 software. According to the Box Behnken test design principle, the factors that visibly affect the microencapsulation EE were selected: SA concentration (A), $CaCl_2$ concentration (B), core wall ratio (C), pH (D) as the independent variable, with the response value of the EE evaluation index.

Structural characterization of microcapsules

Scanning Electron Microscope (SEM) assay

The morphology of LBLF and M-LBLF were characterized by SEM (JSM-7500F, JEOL, Japan). After gold sputtering under an argon atmosphere, the samples were analyzed at 20 kV acceleration voltage.

FT-IR assay

The FT-IR studied the interactions between SA, CS, LBLF and M-LBLF and the encapsulated bioactive substance. The spectrums were conducted on a Spectrum Two spectrophotometer (Perkin Elmer, America), in the wavelength range between 400 and 4000 cm^{-1}. On average, the obtained spectra for each sample were 32 scans at a resolution of 0.5 cm^{-1}.

XRD assay

XRD analyses were performed to research the amorphous or crystalline SA, CS, CS-SA, LBLF and M-LBLF. XRD patterns were acquired on a Bruker AXS D8 Advance (Bruker Inc., Germany) at 40 kV and 30 mA. The patterns were collected at the angle of 5° ~ 80° with a step size of 0.02°.

DSC assay

The thermal behavior of the SA, CS, CS-SA, LBLF and M-LBLF physical mixture, microcapsules were carried out using DSC (Setaram, France). The sample was heated on an aluminum pan from 100°C ~ 400°C at a rate of 10 °C/min under the protection of a nitrogen atmosphere.

Simulated digestion and release of M-LBLF in vitro

In vitro release measurement

The stability of LBLF and M-LBLF were evaluated in simulated oral fluid (SOF), gastric fluid (SGF) and intestinal fluid (SIF) (Wang et al., 2019). The digestive juice solutions were prepared as follows: (1) KH_2PO_4 (0.038 g), Na_2HPO_4 (0.478 g), α-amylase (0.02 g) and NaCl (1.60 g) were dissolved in 200 mL deionized water to form SOF, and the pH was adjusted to 6.75 with phosphate buffer (Jara-Palacios et al., 2018); (2) SGF was prepared by dissolving 4.375 g NaCl and 0.8 g pepsin in 250 mL deionized water (pH=1.2) (Corrêa et al., 2017); (3) 0.268 g tryptase and 1.714 g bile were dissolved in 200 mL of 0.2 M $NaHCO_3$ solution to obtain SIF (Bouayed et al., 2011). In SOF, SGF and SIF, LBLF and M-LBLF in distilled water were incubated at 37°C with the sample collection at 0 min, 30 min, 60 min, 90 min, 120 min, 150 min, 180 min, 210 min, and 240 min. The samples were centrifuged to get the supernatant to determine the TFC.

Releases detection of main monomers from M-LBLF during *in vitro* digestion

Preparation of standard solution

Accurately weighing rutin, caffeic acid, quercetin, *p*-coumarin, kaempferol, ferulic acid and chlorogenic acid standard samples were formulated into 1 mg/mL. Preparation of standard and mixed standard accurately absorbed the above standard to prepare 0.1 mg/mL, stored at 4°C and filtered by 0.22 μm filter membrane.

Chromatographic condition

The separation was performed on an InertSIL-ODS-3 (C18) column (250 mm × 4.6 mm, particle size 5 μm). The injection volume of sample was 20 μL. The mobile phase consisted of methanol (solvent A) and 1% (*v*/*v*) acetic acid in water (solvent B) and flowed at a rate of 1 mL/min. The elution gradient was performed as follows: 0~8 min, 15~20% A; 8~18 min, 20~60% A; 18~25 min, 60% A; 25~30 min, 60~80% A; 30~40 min, 80% A; 40~50 min, 80~15% A; 50~55 min, 15% A, the column temperature was 30°C.

The standard curve was drawn with the mass concentration (mg/mL) as the abscissa and the peak area as the ordinate. To determine the concentration of monomers in flavonoids, the average peak area of each monomer was substituted into the regression equation (Liu et al., 2021) and the content of each monomer was calculated using the formula below (Equation 2):

$$X = \frac{X \times V}{M} \times 1000 \quad (2)$$

Where X is the content of flavonoids (mg/g); Y is the mass concentration of flavonoids in the sample calculated according to the standard curve equation (mg/mL); V is constant volume (mL); M is the sample mass (mg).

2.3 Statistical analysis methods

The results were expressed as mean ± standard deviation (SD). One-way significance analysis (ANOVA) and Turkey test were used to assess the statistical significance (SPSS 17.0 software). $p < 0.05$ was considered as a significant difference. Origin 2022 and Excel 2019 were used for drawing graphics. All experiments were performed in triplicate.

3 Results and discussion

3.1 Microencapsulation of LBLF

M-LBLF preparation

In the single factor experiments, the optimized process condition were SA concentration 0.02 g/mL, CS concentration 0.02 g/mL, $CaCl_2$ concentration 0.05 g/mL, core wall ratio 1:2, drying temperature of freeze-drying 30°C. Based on the single factor experiments and Placket Burman test, the factors that had an apparent influence on EE of LBLF were selected: A (SA concentration), B ($CaCl_2$ concentration), C (core wall ratio) and D (pH) were used as independent variables and EE was used as the response value of the index. A four-factor and three-level response surface analysis were designed and the experiment scheme and the results were shown in Table 1. Using Design Expert 11 software, the simulation equations of M-LBLF EE and dependent variables obtained quadratic response surface multi-regression equation fitted according to the least square method (Equation 3):

$$Y = 90.56 - 0.35 \times A + 0.59 \times B - 0.73 \times C - 0.16 \times D - 0.43 \times AB + 0.90 \times AC + 0.67 \times AD + 0.011 \times BC - 0.22 \times BD + 0.77 \times C \times D - 2.79 \times A^2 - 2.50 \times B^2 - 2.36 \times C^2 - 2.97 \times D^2 \quad (3)$$

Where Y is the predicted EE value of M-LBLF.

Table 1. Design and result analysis for response surface test.

Testing order number	A	B	C	D	EE (%)
1	1	0	0	0	90.51
2	1	-1	0	0	83.43
3	-1	0	-1	0	85.86
4	0	0	0	0	90.55
5	-1	-1	0	0	83.86
6	1	0	0	1	84.61
7	0	-1	1	0	84.43
8	1	0	1	0	86.26
9	1	0	-1	0	84.50
10	0	1	0	1	85.04
11	0	0	0	0	90.82
12	-1	0	1	0	83.90
13	0	0	-1	1	86.79
14	0	0	0	0	90.53
15	0	-1	0	1	85.03
16	-1	1	0	0	83.79
17	0	0	0	0	89.82
18	0	0	1	1	86.44
19	0	-1	-1	0	86.86
20	0	1	-1	0	84.19
21	0	1	0	-1	85.52
22	0	1	1	0	85.88
23	0	0	1	0	83.93
24	-1	0	0	-1	84.02
25	0	0	-1	-1	85.98
26	-1	0	0	1	83.63
27	1	1	0	0	85.86
28	1	0	0	-1	87.12
29	0	-1	0	-1	84.51

As seen in Table 2, the model was highly significant ($p < 0.01$). Critically, lack-of-fit ($p > 0.05$) had no significance. R^2 (98.10%) exceeded 95%, signifying that the established empirical model matched the experiments well and can be employed to predict the outcome with minimal error. According to the *p*-value, the order of factors from most impactful to least was: C> D> A> B. It was shown that the two linear parameters (CD) and their interaction were highly significant ($p < 0.01$) (Dahmoune et al., 2015).

The optimal process ratio obtained from the response surface was as follows: Concentration of SA was 0.025 g/mL, the concentration of $CaCl_2$ was 0.053 g/mL, the core wall ratio was 1:3.2, pH was 6.98, and the highest EE was 90.77% (Figure 1). The EE of the prepared M-LBLF was 90.22%, and the difference from the theoretical value predicted by the model was less than 1%. It showed that the response surface prediction model could predict the EE of M-LBLF well.

Physicochemical analysis of M-LBLF

TFC of the obtained LBLF was 810.88±0.72 mg/g, and the EE of M-LBLF was 90.22±1.67% under the optimal embedding conditions. The static angle of the slug was 36.13° < 40°, indicating that the microcapsules had more fluidity and could meet the

Table 2. Coefficient significance test and variance analysis of regression equation.

Source	Degree of freedom	Sum of squares of deviations	Mean square	*F* value	*P* value	Significant
Mode	41.76	1	2.98	36.53	< 0.0001	**
A: SA concentration	5.62	1	5.62	68.79	< 0.0002	**
B: $CaCl_2$ concentration	2.12	1	2.12	25.92	0.0002	**
C: Core wall ratio	3.55	1	3.55	43.52	< 0.0001	**
D: pH	1.47	1	1.47	18.00	< 0.0001	**
AB	1.21	1	1.21	2.70	0.1226	
AC	3.59	1	3.59	8.01	0.0133	*
AD	0.29	1	0.29	3.51	0.0422	*
BC	4.24	1	4.24	9.47	0.0082	**
BD	0.25	1	0.25	0.56	0.4700	
CD	0.33	1	0.33	4.05	0.0339	*
A^2	16.22	1	16.22	198.57	< 0.0001	**
B^2	12.39	1	12.39	151.79	< 0.0001	**
C^2	6.73	1	6.73	82.41	< 0.0001	**
D^2	7.95	1	7.95	97.40	< 0.0001	**
Remant	1.14	14	0.08			
Lack of fit	0.93	10	0.09	1.70	0.3211	
Pure Error	0.22	4	0.05			
Sum	42.90	28				
R^2 = 0.9810; R^2_{Adj} = 0.9620; Model precision = 24.4593						

*Indicates significant $p < 0.05$. **Indicates significant $p < 0.01$. The determination coefficient $R^2 = 0.9810$, the correction coefficient $R^2_{Adj} = 0.9620$, indicating that the regression equation fits well with the actual experiments, which can be used to determine the optimal preparation conditions.

application requirements. The microencapsulation promoted the dissolution of LBLF with an average particle size of 623.0±2.11 μm, and the solubility in water was increased nearly 40 times.

3.2 Structural characterization of M-LBLF

M-LBLF morphology analysis

SEM demonstrated that the microcapsules were almost spherical, and LBLF was entrapped within SA and CS polymeric matrices. As shown in Figure 2a, LBLF not only had a regular fragment crystal in micromorphology but possessed a relatively loose structure. The wet microcapsules prepared by the polyelectrolyte cross-linking method exhibited smooth and completed granules with uniform distribution (Figure 2b). The microcapsules were generally spherical but accompanied by elliptic, cylindrical, granulated, flocculent, and irregular shapes and showed an inconsistent surface morphology, smooth, folded and sunken (Lei et al., 2018). Moreover, the internal structure of M-LBLF viewed at 1 μm was a clear crystal block (Figure 2c). It was suggested that the M-LBLF surface was close to the spherical structure, and most of the surfaces were smooth with complete capsule walls, which displayed a closely connected rough and dense structure (Figure 2d). There were pores and numerous voids on the surface of M-LBLF, which might be caused by the water loss in the process of vacuum freeze-drying (Cruz et al., 2019).

FT-IR, XRD and DSC analysis

The intermolecular interactions within the microcapsules were observed by FT-IR (Figure 3a). The FT-IR spectrum of SA showed peaks at 3415 cm^{-1}, 2931 cm^{-1}, 1633 cm^{-1}, 1158 cm^{-1} and 884 cm^{-1}, corresponding to the stretching vibration of O-H, C-H, COOH, O-H and C-O-C group. Nevertheless, the intense vibrational band at 2931 cm^{-1} and 2863 cm^{-1} were ascribed to the C-H stretching vibration (Tian et al., 2022). Symmetrical and asymmetrical stretching vibrations of primary amine -NH_2 gave a signal at 1633 cm^{-1}. For the characteristic spectrum of CS: the characteristic peak at 1158 cm^{-1} corresponded to O-C-O stretching vibration, and the peak at 1075 cm^{-1} situated the CS stretching vibration (Yousefi et al., 2020). The characteristic peak of LBLF was 3415 cm^{-1}, which could be connected to the O-H of flavonoids or bound water that had not been completely removed. A stretching vibration of the aliphatic -CH_2 peak was in the 2863 cm^{-1}. The stretching vibration of C=O appeared at 1633 cm^{-1}, and 1124 cm^{-1} and 652 cm^{-1} could be related to the stretching vibration of C-O in primary alcohols. In the M-LBLF spectrum, the peak of SA, CS and LBLF had not disappeared, indicating electrostatic interaction between physical electrostatic interaction and no new chemical bonds. Nonetheless, an extra characteristic peak at 1735 cm^{-1} might be contributed by electrostatic complexation between SA and CS (Li et al., 2020). FT-IR showed that LBLF had been successfully embedded in microcapsules, which was beneficial in relieving LBLF from oxidation and denaturation.

Figure 3b displayed the XRD for core and wall materials and M-LBLF. The XRD spectrum of the CS and SA indicated an amorphous polymeric structure with high crystallinity founded by a broad peak around 2θ of about 20°. LBLF produced a broad peak at 2θ = 40.6°, indicating LBLF had existence in the crystalline form. Compared with CS, SA and CS-SA, M-LBLF displayed a reduction in peak intensity and broadness to various degrees, suggesting the structural destruction of CS and SA in the microcapsules, which might be attributed to the ionic interaction-induced modification of the molecular arrangement in the crystal lattice (Tang et al., 2022). The diffraction peak positions of M-LBLF and LBLF were the same, but there were changes at 2θ = 36°, 40.6° and 51.8° due to microencapsulation that converts the amorphous structural part to a crystalline state

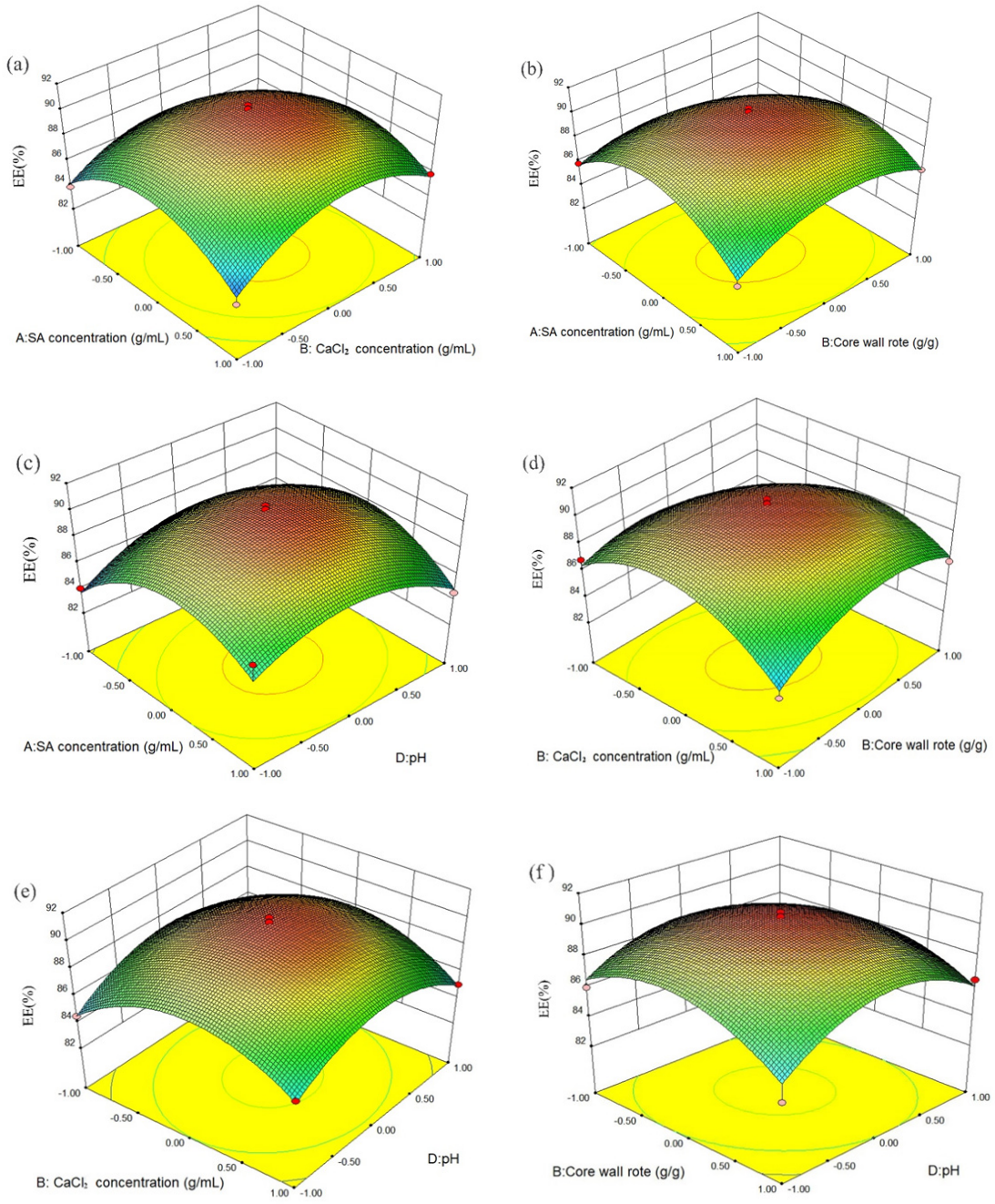

Figure 1. Response surface curves of the interaction effects of SA, CS, core wall ratio and pH on the encapsulation efficiency (EE) of M-LBLF. (a) $CaCl_2$ and SA; (b) core wall ratio and SA; (c) core wall ratio and $CaCl_2$; (d) pH and SA; (e) pH and $CaCl_2$; (f) pH and core wall ratio.

(Gavalyan, 2016; Duman & Kaya, 2016). As shown in the XRD pattern, a rise in the sample's crystallinity was explained by an improvement in the sharpness of the diffraction peaks. It also proved to have good stability in the M-LBLF (Liao et al., 2017).

As shown in Figure 3c, DSC could characterize the amorphous properties of the sample (Gandhi et al., 2014). In this study, DSC was performed to examine the thermal behavior crystallization of CS, SA, CS-SA, LBLF and M-LBLF. All the samples displayed a distinct endothermic peak between 250 and 400°C, confirming denaturation and moisture loss (Guarienti et al., 2021). M-LBLF had a wider and higher exothermic peak than the SA and CS, ascribed to a change of energy induced by the electrostatic interaction between wall materials (Hu et al., 2018). On the other hand, the exothermic peak of CS at about 300.90°C revealed CS's depolymerization and thermal decomposition. The exothermic peak of LBLF at 305.96°C was related to the melting of flavonoids, which corresponded to the glass transition temperature of LBLF (Sansone et al., 2011). The glass transition temperature of M-LBLF (378.44°C) was much higher than that of LBLF (305.96°C) because SA and CS showed preferable thermal stability of microencapsulation.

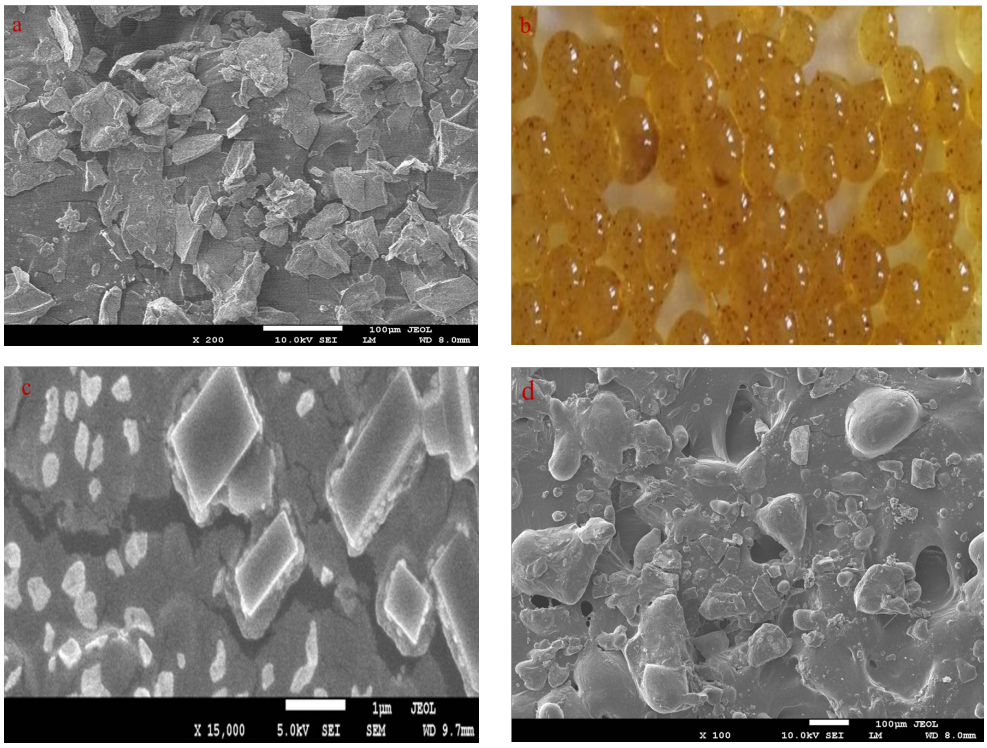

Figure 2. SEM images of LBLF and M-LBLF. (a) SEM image of freeze-dried LBLF (magnification: 200×); (b) The photograph of M-LBLF in the wet state; (c) SEM image of M-LBLF (magnification: 15000×); (d) SEM images of M-LBLF (magnification: 100×). SEM is abbreviation of scanning electron microscope.

3.3 Stability of M-LBLF during the simulated digestion in vitro

As shown in Table 3, the potential ability of M-LBLF to control LBLF release was evaluated in the simulated SGF as valuable strategy to improve the bioavailability of LBLF. It could be seen that there were no significant differences between the release degrees of M-LBLF in the simulated SOF ($p > 0.05$). This demonstrated that the release of flavonoids was effectively controlled by the wall materials (SA and CS). After SGF for 3 h, the release amounts of flavonoid from LBLF and M-LBLF were 75.74±1.08% and 44.13±0.99%. Such results manifested that the structural stability of the wall material protected the core material well under the acidic condition of simulated gastric juice; microencapsulation improved the flavonoid stability and had an excellent sustained-release effect (Kumar et al., 2017). It has been documented that microencapsulation modified the structure of the sample to change the release rate (Flores et al., 2015). Therefore, M-LBLF showed higher resistance to the acidic environment, the preservation rate of flavonoid compounds was improved and more than 1/2 of the flavonoid compounds entered the intestinal environment (Hu et al., 2018).

During simulated SIF, the release of unencapsulated flavonoids in LBLF increased significantly within 0~3 h and tended to be stable, indicating that flavonoids were not fully released during SGF and SIF continued to promote flavonoid release. In SIF from 0 to 3 h, the release of flavonoids in microcapsules was dramatically improved ($p < 0.05$) with the prolongation of time points ($p < 0.05$). It was manifested that M-LBLF had good enteric solubility since the polyelectrolyte membrane formed by the electrostatic interaction of CS and SA was sensitive to the pH value of the environment. The release amount of wrapped material was different under different pH conditions, so the accurately targeted release of the core material could be realized by controlling the pH value (Ahmad et al., 2019). Microencapsulation could effectively prevent the release of flavonoids under gastric conditions and improve their bioavailability by reducing the chemical degradation of flavonoids in the intestinal environment. It shows that microencapsulation played a slow-release effect on flavonoids in the process of SGF and was released in large quantities during SIF, which was conducive to the release of phenolic substances.

Monomers released from M-LBLF during the simulated digestion in vitro

The change of main monomers in plant extracts was related to the change in TFC and antioxidant activity (Ambigaipalan et al., 2017). The major monomers of M-LBLF were examined using High-Performance Liquid Chromatography to identify any alterations that occurred during *in vitro* digestion (Figure 4). Seven monomers were identified in M-LBLF, including four phenolic acids (chlorogenic acid, caffeic acid, *p*-coumaric acid and ferulic acid) and three flavonoids (rutin, quercetin and karmatol), which have been reported in *Lycium barbarum* L. leaves previously (Vinholes et al., 2018). Compared with no embedding LBLF, the main monomers component did not change significantly in SOF, composition and main monomers in SGF had a significant change (the SGF was on the decline, was on the rise in SIF), showing that most of the monomers in the process of the SGF

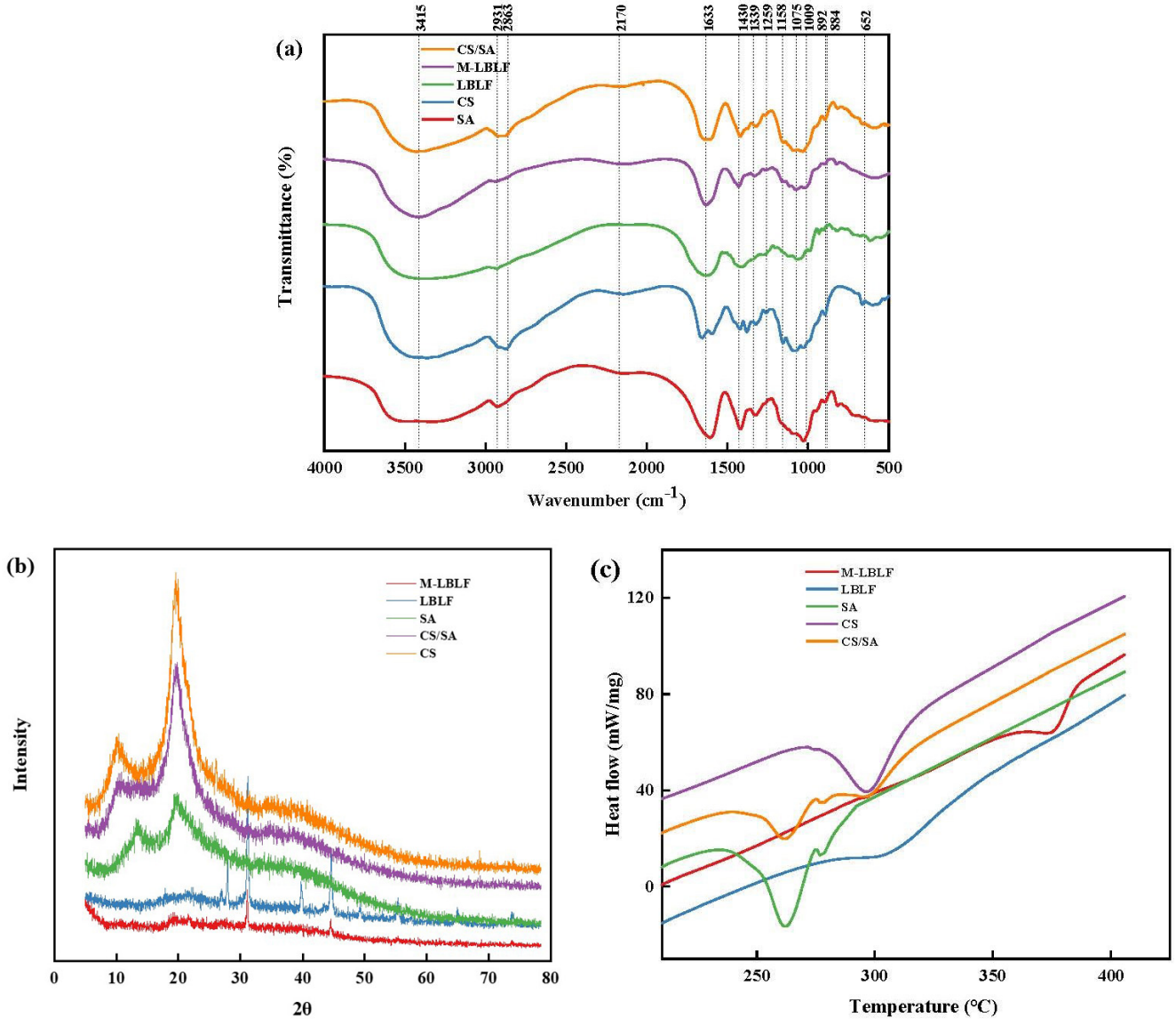

Figure 3. FT-IR, XRD and DSC spectra of SA, CS, LBLF and M-LBLF. Characterization of structural stability of microcapsules, the stability of M-LBLF, LBLF, SA, CS and CS/SA were determined. (a) FT-IR analysis at the wavenumber range of 400-4000 cm^{-1}. The five samples were separately grounded with potassium chloride. (b) XRD spectra at the scan range from 5° to 78°. (c) DSC analysis was performed to examine the thermal stability of M-LBLF between 203°C and 405°C. FT-IR is the abbreviation of transform infrared spectroscopy, XRD is the abbreviation of X-ray diffraction and DSC is the abbreviation of differential scanning calorimetry.

Table 3. Flavonoids release (%) of M-LBLF during *in vitro* simulated digestion.

Stages	Samples	Digestion time (min)							
		30	60	90	120	150	180	210	240
SOF	M-LBLF	1.90 ± 2.50^{g}	2.78 ± 2.16^{e}	2.44 ± 1.25^{f}	2.43 ± 1.66^{f}	2.85 ± 0.49^{d}	3.2 ± 0.45^{c}	3.35 ± 1.66^{b}	3.62 ± 1.33^{a}
	LBLF	1.72 ± 0.72^{c}	3.52 ± 0.42^{b}	4.09 ± 0.58^{b}	6.89 ± 0.43^{f}	7.33 ± 1.55^{a}	7.35 ± 0.76^{a}	7.32 ± 0.72^{a}	7.05 ± 1.87^{a}
SGF	M-LBLF	4.23 ± 1.14^{e}	5.49 ± 0.57^{e}	9.85 ± 0.99^{d}	23.5 ± 0.75^{f}	37.31 ± 2.28^{b}	44.13 ± 0.99^{a}	44.29 ± 0.57^{a}	44.31 ± 2.15^{a}
	LBLF	10.58 ± 1.08^{g}	31.11 ± 2.15^{f}	45.26 ± 2.85^{e}	49.57 ± 1.87^{d}	67.65 ± 2.85^{c}	75.74 ± 1.08^{b}	76.98 ± 1.87^{ab}	77.15 ± 1.21^{a}
SIF	M-LBLF	9.33 ± 0.75^{f}	10.57 ± 1.20^{f}	24.26 ± 0.57^{e}	39.8 ± 0.53^{d}	75.87 ± 1.27^{c}	83.33 ± 2.08^{b}	85.90 ± 1.25^{a}	85.88 ± 0.72^{a}
	LBLF	9.64 ± 2.85^{f}	27.74 ± 2.85^{e}	34.05 ± 2.85^{d}	48.51 ± 3.73^{c}	62.44 ± 2.85^{b}	74.98 ± 2.85^{a}	76.60 ± 0.75^{a}	77.01 ± 0.36^{a}

Different superscripts in the same row with small letters are significantly different ($p < 0.05$). Each value is mean ± SD of triplicate measurements.

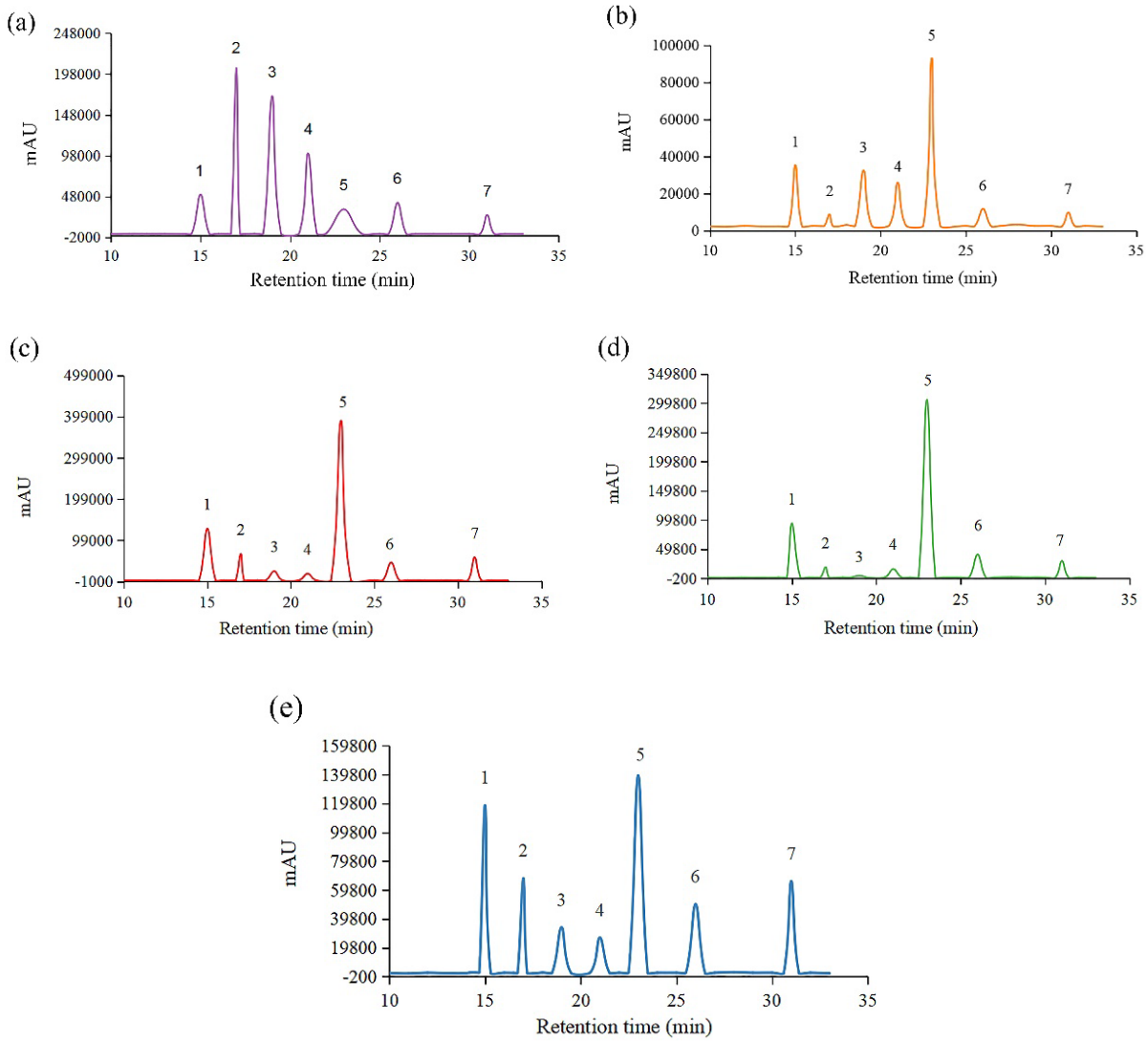

Figure 4. HPLC profiles of M-LBLF at different stages during *in vitro* digestion. According to the spectra of mixed standard (a), the seven monomers from M-LBLF correspond to 1 ~ 7, attributing to chlorogenic acid, caffeic acid, *p*-coumarin and ferulic acid, rutin, quercetin and kaempferol respectively. The main monomers were detected by HPLC in undigested M-LBLF (b), and during the simulated oral digestion (c), gastric digestion (d) and intestinal digestion (e). HPLC is the abbreviation of high-performance liquid chromatography.

degradation or conversion (Yousefi et al., 2020). The content changes of main monomer substances in microcapsules were quantitatively analyzed, as shown in Table 4 and Figure 4. During SOF, the main monomers decreased by 8.50%, 6.91%, 6.70%, 3.34%, 7.36%, 1.34% and 5.50%, respectively, phenolic acids were more stable than flavonoids in SOF (Zang et al., 2022). In SGF stage, the seven monomers' changes were 2.6%, 34.03%, 37.21%, 61.53%, 12.47%, 45.39% and 18.37%, respectively, and the two monomers with the highest content of rutin and chlorogenic acid were significantly decreased. The binding of flavonoids to pepsin reduces the concentration of flavonoids in the low-pH solution (Liović et al., 2020). In SIF, the main contents of the monomer were rising. Due to the Trypsin releasing some protein-bound phenolic compounds, the reduction of food particle size also facilitates the release of phenolic compounds. In addition, some phenolic substances were released from the matrix at neutral pH conditions.

4 Conclusion

This study used polyelectrolyte crosslinking combined with freeze-drying technology to LBLF in SA and CS to form M-LBLF. Topography observations showed that the surface of the microcapsules was densely porous and irregularly shaped. Structural characterization showed that there were characteristic absorption peaks in the core and the wall of the capsules. It was proved that the microencapsulation of M-LBLF had a specific influence on the crystalline properties of LBLF, and improved the thermal stability of LBLF. The results of simulated digestion *in vitro* showed that microencapsulation could significantly enhance the stability of LBLF in SIF and play a role in sustained release. It was conducive to the in-depth development and application of *Lycium barbarum* L. leaves.

Considering the potential healthcare benefits of LBLF, primary processing products such as *Lycium barbarum* L. leaves tea are the

Table 4. Changes in the release of the main monomers from M-LBLF during the different digestion stages *in vitro*

Stages	Time (min)	Monomer content (mg/g)						
		chlorogenic acid	caffeic acid	*p*-coumaric acid	ferulic acid	rutin	quercetin	kaempferol
SOF	0	44.03 ± 0.86[a]	6.55 ± 0.72[a]	3.72 ± 0.16[a]	2.83 ± 0.41[a]	107.52 ± 0.67[a]	2.10 ± 0.10[a]	4.60 ±0.52[a]
	30	44.01 ± 0.96[a]	6.65 ± 1.06[a]	3.76 ± 0.15[a]	2.93 ± 0.49[a]	106.33 ± 2.22[a]	2.12 ± 0.19[a]	4.60 ± 1.52[a]
	60	44.77 ± 0.62[a]	6.15 ± 0.26[a]	3.79 ± 0.01[a]	2.99 ± 0.31[a]	107.92 ± 1.85[a]	2.13 ± 0.16[a]	4.67 ± 0.26[a]
	90	44.77 ± 1.31[a]	6.15 ± 0.75[a]	3.19 ± 0.06[a]	2.99 ± 0.43[a]	107.92 ± 2.80[a]	2.23 ± 0.23[a]	4.67 ± 0.61[a]
	120	43.81 ± 1.53a	5.96 ± 0.52[a]	3.79 ± 0.51[a]	2.97 ± 0.28[a]	105.22 ± 2.80[a]	1.81 ± 0.34[a]	4.39 ± 0.94[a]
	150	43.49 ± 1.64[a]	6.00 ± 0.93[a]	3.79 ± 0.20[a]	2.96 ± 0.34[a]	102.39 ± 2.52[a]	1.85 ± 0.09[a]	4.05 ± 0.60[a]
	180	42.70 ± 1.34[a]	5.94 ± 1.32[a]	3.80 ± 0.33[a]	2.96 ± 0.11[a]	103.09 ± 0.22[a]	1.96 ± 0.06[a]	4.15 ± 0.43[a]
	210	42.57 ± 1.82[a]	5.95 ± 0.85[a]	3.79 ± 0.27[a]	2.99 ± 0.31[a]	107.92 ± 4.64[a]	1.93 ± 0.01[a]	4.07 ± 0.39[a]
	240	42.11 ± 1.66[a]	6.02 ± 0.52[a]	3.78 ± 0.41[a]	2.95 ± 0.46[a]	106.05 ± 3.93[a]	1.83 ± 0.05[a]	3.87 ± 0.26[a]
SGF	30	31.84 ± 0.83[a]	0.95 ± 0.71[b]	0.54 ± 0.06[a]	0.20 ± 0.08[b]	87.73 ± 4.74[a]	0.89 ± 0.02[a]	1.60 ± 0.32[b]
	60	30.16 ± 0.51[b]	1.30 ± 0.44[a]	0.74 ± 0.02[a]	0.34 ± 0.04[b]	86.34 ± 1.57[c]	1.40 ± 0.06[a]	1.94 ± 0.32[a]
	90	30.76 ± 0.67[b]	1.09 ± 0.52[b]	0.79 ± 0.07[a]	0.60 ± 0.06[a]	84.73 ± 3.92[a]	1.41 ± 0.08[a]	1.92 ± 0.11[a]
	120	30.69 ± 1.02[b]	1.42 ± 0.54[a]	0.79 ± 0.03[a]	0.38 ± 0.01[b]	82.66 ± 3.26[ab]	1.67 ± 0.05[a]	1.98 ± 0.13[a]
	150	30.70 ± 0.78[b]	1.44 ± 0.76[a]	0.70 ± 0.00[a]	0.46 ± 0.02[a]	81.09 ± 2.24[b]	1.96 ± 0.01[a]	2.15 ± 0.19[a]
	180	31.02 ± 0.86[a]	1.39 ± 0.18[a]	0.89 ± 0.17[a]	0.53 ± 0.03[a]	83.81 ± 2.60[a]	1.46 ± 0.02[a]	2.06 ± 0.21[a]
	210	31.03 ± 0.52[a]	1.37 ± 0.24a	0.89 ± 0.32[a]	0.52 ± 0.06[a]	81.94 ± 3.15[d]	1.61 ± 0.08[a]	1.99 ± 0.17[a]
	240	30.99 ± 0.73[b]	1.44 ± 0.39[a]	0.86 ± 0.79[a]	0.52 ± 0.05[a]	78.87 ± 2.78[c]	1.63 ± 0.03[a]	1.96 ± 0.16[a]
SIF	30	46.76 ± 0.95[b]	5.09 ± 0.50[b]	7.29 ± 0.16[a]	2.86 ± 0.43[a]	106.73 ± 3.87[b]	4.41 ± 0.06[a]	4.62 ± 0.15[a]
	60	49.26 ± 3.83[a]	5.37 ± 0.61[b]	3.13 ± 0.11[b]	2.82 ± 0.35[a]	123.42 ± 3.37[a]	2.28 ± 0.05[b]	4.44 ± 0.13a
	90	44.77 ± 2.51[b]	6.15 ± 1.17[a]	3.19 ± 0.14[b]	2.99 ± 0.71[a]	107.92 ± 0.88[b]	2.23 ± 0.09[b]	4.67 ± 0.21[a]
	120	43.99 ± 3.14[bc]	5.10 ± 0.37[b]	2.99 ± 0.96[b]	2.66 ± 0.84[a]	125.39 ± 0.96[a]	1.85 ± 0.16[c]	4.35 ± 0.34[a]
	150	44.81 ± 2.60[b]	5.66 ± 0.96[b]	2.99 ± 0.47[b]	2.77 ± 0.34[a]	125.22 ± 1.18[a]	1.81 ± 0.24[c]	4.39 ± 0.15[a]
	180	43.66 ± 2.75[c]	5.96 ± 0.88[a]	2.83 ± 0.23[b]	2.58 ± 0.25[a]	121.26 ± 0.61[a]	2.17 ± 0.06[b]	4.10 ± 0.96[a]
	210	42.70 ± 3.26[c]	5.44 ± 0.56[b]	2.70 ± 0.26[b]	2.46 ± 0.29[a]	123.09 ± 2.50[a]	1.96 ± 0.31[c]	4.15 ± 0.41[a]
	240	41.83 ± 2.43[d]	5.17 ± 0.42[b]	3.09 ± 0.35[b]	2.80 ± 0.31[a]	126.94 ± 3.39[a]	1.91 ± 0.29[c]	4.46 ± 0.28[a]

Different superscripts in the same row with small letters are significantly different ($p < 0.05$). Each value is mean ± SD of triplicate measurements.

common products on the market. In this paper, we extensively investigate the preparation of M-LBLF and the improving strategy for its stability. Microencapsulation can also prolong the validity of the active ingredients in *Lycium barbarum* L. leaves, which can lay a foundation for expanding the application of *Lycium barbarum* L. leaves and developing related healthy food.

Acknowledgements

This work was supported by National Natural Science Foundation of China (32160534), Natural Science Foundation Project of Ningxia (2022AAC03018), and Ningxia Key Research and Development Program Grant (2022BBF03016).

References

Ahmad, M., Mudgil, P., Gani, A., Hamed, F., Masoodi, F. A., & Maqsood, S. (2019). Nano-encapsulation of catechin in starch nanoparticles: characterization, release behavior and bioactivity retention during simulated *in-vitro* digestion. *Food Chemistry*, 270, 95-104. http://dx.doi.org/10.1016/j.foodchem.2018.07.024. PMid:30174096.

Ambigaipalan, P., Camargo, A. C., & Shahidi, F. (2017). Identification of phenolic antioxidants and bioactive of pomegranate seeds following juice extraction using HPLC-DAD-ESI-MSN. *Food Chemistry*, 221, 1883-1894. http://dx.doi.org/10.1016/j.foodchem.2016.10.058. PMid:27979177.

Bouayed, J., Hoffmann, L., & Bohn, T. (2011). Total phenolics, flavonoids, anthocyanins and antioxidant activity following simulated gastrointestinal digestion and dialysis of apple varieties: bioaccessibility and potential uptake. *Food Chemistry*, 128(1), 14-21. http://dx.doi.org/10.1016/j.foodchem.2011.02.052. PMid:25214323.

Cao, Y., Xie, L., Liu, K., Liang, Y., Dai, X., Wang, X., Lu, J., Zhang, X., & Li, X. (2021). The antihypertensive potential of flavonoids from Chinese herbal medicine: a review. *Pharmacological Research*, 174, 105919. http://dx.doi.org/10.1016/j.phrs.2021.105919. PMid:34601080.

Chen, J. H., Kou, T. T., Fan, Y. L., & Niu, Y. H. (2020). Antioxidant activity and stability of the flavonoids from Lycium barbarum leaves during gastrointestinal digestion in vitro. *International Journal of Food Engineering*, 16(7), 20190315. http://dx.doi.org/10.1515/ijfe-2019-0315.

Corrêa, R. C. G., Haminiuk, C. W. I., Barros, L., Dias, M. I., Calhelha, R. C., Kato, C. G., Correa, V. G., Peralta, R. M., & Ferreira, I. C. F. R. (2017). Stability and biological activity of Merlot (Vitis vinifera) grape pomace phytochemicals after simulated in vitro gastrointestinal digestion and colonic fermentation. *Journal of Functional Foods*, 36, 410-417. http://dx.doi.org/10.1016/j.jff.2017.07.030.

Cruz, M. C., Dagostin, J. L., Perussello, C. A., & Masson, M. L. (2019). Assessment of physicochemical characteristics, thermal stability and release profile of ascorbic acid microcapsules obtained by complex coacervation. *Food Hydrocolloids*, 87, 71-82. http://dx.doi.org/10.1016/j.foodhyd.2018.07.043.

Dahmoune, F., Nayak, B., Moussi, K., Remini, H., & Madani, K. (2015). Optimization of microwave-assisted extraction of polyphenols from Myrtus communis L. leaves. *Food Chemistry*, 166, 585-595. http://dx.doi.org/10.1016/j.foodchem.2014.06.066. PMid:25053097.

Duman, F., & Kaya, M. (2016). Crayfish chitosan for microencapsulation of coriander (Coriandrum sativum L.) essential oil. *International Journal of Biological Macromolecules*, 92, 125-133. http://dx.doi.org/10.1016/j.ijbiomac.2016.06.068. PMid:27341783.

Feng, X., Gou, K., Yang, C., Li, J., Chen, H., & Liu, X. (2019). Growth and fruit production of tomato grafted onto wolfberry (Lycium chinense) rootstock in saline soil. *Scientia Horticulturae*, 255, 298-305. http://dx.doi.org/10.1016/j.scienta.2019.05.028.

Flores, F. P., Singh, R. K., Kerr, W. L., Phillips, D. R., & Kong, P. B. (2015). In vitro release properties of encapsulated blueberry (Vaccinium ashei). *Food Chemistry*, 168, 225-232. http://dx.doi.org/10.1016/j.foodchem.2014.07.059. PMid:25172704.

Gandhi, A., Jana, S., & Sen, K. K. (2014). In-vitro release of acyclovir-loaded Eudragit RLPO® nanoparticles for sustained drug delivery. *International Journal of Biological Macromolecules*, 67, 478-482. http://dx.doi.org/10.1016/j.ijbiomac.2014.04.019. PMid:24755259.

Gavalyan, V. B. (2016). Synthesis and characterization of new chitosan-based Schiff Base compounds. *Carbohydrate Polymers*, 145, 37-47. http://dx.doi.org/10.1016/j.carbpol.2016.02.076. PMid:27106149.

Guarienti, C., Bender, L. E., Frota, E. G., Bertolin, T. E., Costa, J. A. V., & Richards, N. S. P. S. (2021). Effects of microencapsulation on the preservation of thermal stability and antioxidant properties of Spirulina. *Journal of Food Measurement and Characterization*, 15(6), 5657-5668. http://dx.doi.org/10.1007/s11694-021-01140-0.

Hiew, C. W., Lee, L. J., Junus, S., Tan, Y. N., Chai, T. T., & Ee, K.-Y. (2022). Optimization of microwave-assisted extraction and the effect of microencapsulation on mangosteen (Garcinia mangostana L.) rind extract. *Food Science and Technology*, 42, e35521. http://dx.doi.org/10.1590/fst.35521.

Hu, Y., Li, Y., Zhang, W. L., Kou, G. N., & Zhou, Z. Q. (2018). Physical stability and antioxidant activity of citrus flavonoid in arabic gum-stabilized microcapsules: modulation of whey protein concentrate. *Food Hydrocolloids*, 77, 588-597. http://dx.doi.org/10.1016/j.foodhyd.2017.10.037.

Huang, T., Qin, K., Yan, Y. M., He, X. R., Dai, G. L., & Zhang, B. (2022). Correlation between the storability and fruit quality of fresh goji berries. *Food Science and Technology*, 42, e46120. http://dx.doi.org/10.1590/fst.46120.

Jara-Palacios, M. J., Gonçalves, S., Hernanz, D., Heredia, F. J., & Romano, A. (2018). Effects of in vitro gastrointestinal digestion on phenolic compounds and antioxidant activity of different white wine making by products extracts. *Food Research International*, 109, 433-439. http://dx.doi.org/10.1016/j.foodres.2018.04.060. PMid:29803468.

Kumar, L. R. G., Chatterjee, N. S., Tejpal, C. S., Vishnu, K. V., Anas, K. K., Asha, K. K., Anandan, R., & Mathew, S. (2017). Evaluation of chitosan as a wall material for microencapsulation of squalene by spray drying: characterization and oxidative stability studies. *International Journal of Biological Macromolecules*, 104(Pt B), 1986-1995. http://dx.doi.org/10.1016/j.ijbiomac.2017.03.114. PMid:28342753.

Lei, M., Jiang, F.-C., Cai, J., Hu, S., Zhou, R., Liu, G., Wang, Y. H., Wang, H. B., He, J. R., & Xiong, X. G. (2018). Facile microencapsulation of olive oil in porous starch granules: fabrication, characterization, and oxidative stability. *International Journal of Biological Macromolecules*, 111, 755-761. http://dx.doi.org/10.1016/j.ijbiomac.2018.01.051. PMid:29329810.

Lei, Z., Chen, X., Cao, F., Guo, Q., & Wang, J. (2022). Phytochemicals and bioactivities of Goji (Lycium barbarum L. and Lycium chinense Mill.) leaves and their potential applications in the food industry: a review. *International Journal of Food Science & Technology*, 57(3), 1451-1461. http://dx.doi.org/10.1111/ijfs.15507.

Li, C., Li, B. G., Zhu, C. H., & Meng, X. (2020). Modeling and optimization of tea polyphenol-alginate/chitosan magnetic microcapsules. *Journal of Molecular Structure*, 1208, 127827. http://dx.doi.org/10.1016/j.molstruc.2020.127827.

Liao, X., Yang, X. L., Li, Y., & Ming, J. (2017). Storage stability and antioxidant activity of quercetin microcapsules. *Journal of Agricultural and Food Chemistry*, 38(1), 60-66.

Liović, N., Bilušić, T. R., Jambrak, A., Krešić, G., & Markić, J. (2020). Stability of blueberry polyphenols subjected to in vitro digestion with human gastrointestinal enzymes. *The Proceedings of the Nutrition Society*, 79(OCE2), E240. http://dx.doi.org/10.1017/S0029665120001883.

Liu, R., Chu, X., Su, J., Fu, X., Kan, Q. B., Wang, X. Y., & Zhang, X. Y. (2021). Enzyme-assisted ultrasonic extraction of total flavonoids from Acanthopanax senticosus and their enrichment and antioxidant properties. *Processes*, 9(10), 1708. http://dx.doi.org/10.3390/pr9101708.

Lu, Y., Guo, S., Zhang, F., Yan, H., Qian, D. W., Wang, H. Q., Jin, L., & Duan, J. A. (2019). Comparison of functional components and antioxidant activity of Lycium barbarum L. fruits from different regions in China. *Molecules*, 24(12), 2228. http://dx.doi.org/10.3390/molecules24122228. PMid:31207958.

Magiera, S., & Zaręba, M. (2015). Chromatographic determination of phenolic acids and flavonoids in Lycium barbarum L. and evaluation of antioxidant activity. *Food Analytical Methods*, 8(10), 2665-2674. http://dx.doi.org/10.1007/s12161-015-0166-y.

Mocan, A., Zengin, G., Simirgiotis, M., Schafberg, M., Mollica, A., Vodnar, D. C., Crişan, G., & Rohn, S. (2017). Functional constituents of wild and cultivated Goji (L. barbarum L.) leaves: phytochemical characterization, biological profile, and computational studies. *Journal of Enzyme Inhibition and Medicinal Chemistry*, 32(1), 153-168. http://dx.doi.org/10.1080/14756366.2016.1243535. PMid:28095717.

Oliveira, A. K. S., Silva, A. M. O., Pereira, R. O., Santos, A. S., Barbosa, E. V. Jr., Bezerra, M. T., Barreto, R. S. S., Quintans-Junior, L. J., & Quintans, J. S. S. (2022). Anti-obesity properties and mechanism of action of flavonoids: a review. *Critical Reviews in Food Science and Nutrition*, 62(28), 7827-7848. http://dx.doi.org/10.1080/10408398.2021.1919051. PMid:33970708.

Sansone, F., Mencherini, T., Picerno, P., d'Amore, M., Aquino, R. P., & Lauro, M. R. (2011). Maltodextrin/pectin microparticles by spray drying as a carrier for nutraceutical extracts. *Journal of Food Engineering*, 105(3), 468-476. http://dx.doi.org/10.1016/j.jfoodeng.2011.03.004.

Shang, Y.-F., Zhang, T.-H., Thakur, K., Zhang, J.-G., Cespedes-Acuña, C. L. A., & Wei, Z.-J. (2022). HPLC-MS/MS targeting analysis of phenolics metabolism and antioxidant activity of extractions from Lycium barbarum and its meal using different methods. *Food Science and Technology*, 42, e71022. http://dx.doi.org/10.1590/fst.71022.

Tang, Q., Liu, H. C., Huang, G. C., Yuan, Z., Fu, M. Q., Bu, Z. B., Wen, J., & Xu, X. Y. (2022). The structural characterization, physicochemical properties, and stability of gardenia yellow pigment microcapsules. *Lebensmittel-Wissenschaft + Technologie*, 162, 113507. http://dx.doi.org/10.1016/j.lwt.2022.113507.

Tian, B. R., Cheng, J. H., Zhang, T. P., Liu, Y., & Chen, D. (2022). Multifunctional chitosan-based film loaded with hops β-acids: preparation, characterization, controlled release and antibacterial mechanism. *Food Hydrocolloids*, 124(B), 107337. http://dx.doi.org/10.1016/j.foodhyd.2021.107337.

Vinholes, J., Reis, S. F., Lemos, G., Barbieri, R. L., Freitas, V., Franzon, R. C., & Vizzotto, M. (2018). Correction: effect of in vitro digestion on the functional properties of Psidium cattleianum Sabine (araçá),

Butia odorata (Barb. Rodr.) Noblick (butiá) and Eugenia uniflora L. (pitanga) fruit extracts. *Food & Function*, 9(12), 6380-6390. http://dx.doi.org/10.1039/C8FO01329B. PMid:30457133.

Wang, B., Lv, D., Huang, P., Yan, F., Liu, C., & Liu, H. (2019). Optimization, evaluation and identification of flavonoids in *Cirsium setosu* (Willd.) MB by using response surface methodology. *Journal of Food Measurement and Characterization*, 13(2), 1175-1184. http://dx.doi.org/10.1007/s11694-019-00033-7.

Wen, H., Zhang, D., Liu, J., Shang, X. M., Liu, X. T., Du, Z. Y., & Zhang, T. (2022). Application of γ-cyclodextrin-lysozyme as host materials for encapsulation of curcumin: characterization, stability, and controlled release properties. *Journal of the Science of Food and Agriculture*, 102(13), 5925-5934. http://dx.doi.org/10.1002/jsfa.11943. PMid:35437803.

Yousefi, M., Khanniri, E., Shadnoush, M., Khorshidian, N., & Mortazavian, A. M. (2020). Development, characterization and *in vitro* antioxidant activity of chitosan-coated alginate microcapsules entrapping Viola odorata Linn. extract. *International Journal of Biological Macromolecules*, 163, 44-54. http://dx.doi.org/10.1016/j.ijbiomac.2020.06.250. PMid:32615224.

Zang, Z., Chou, S., Si, X., Cui, H., Tan, H., Ding, Y., Liu, Z., Wang, H., Lang, Y., Tang, S., Li, B., & Tian, J. (2022). Effect of bovine serum albumin on the stability and antioxidant activity of blueberry anthocyanins during processing and in vitro simulated digestion. *Food Chemistry*, 373(Pt B), 131496. http://dx.doi.org/10.1016/j.foodchem.2021.131496. PMid:34836668.

Zhao, X. Q., Guo, S., Yan, H., Lu, Y. Y., Zhang, F., Qian, D. W., Wang, H. Q., & Duan, J. A. (2019). Analysis of phenolic acids and flavonoids in leaves of Lycium barbarum from different habitats by ultra-high performance liquid chromatography coupled with triple quadrupole tandem mass spectrometry. *Biomedical Chromatography*, 33(8), e4552. http://dx.doi.org/10.1002/bmc.4552. PMid:30985939.